Journal of Applied Polymer Science

Clay Distribution and Crystalline Structure Evolution in Polyamide 6/Montmorillonite Composites Prepared by Activated Anionic Polymerization

Nadya Dencheva, Zlatan Denchev
i3N – Institute for Polymers and Composites, University of Minho, Guimarães 4800-058, Portugal
Correspondence to: Z. Denchev (E-mail: denchev@dep.uminho.pt)

ABSTRACT: Nanostructured polymer composites (NPC) based on polyamide 6 (PA6) are prepared by activated anionic ring-opening polymerization (AAROP) of mixtures of ε-caprolactam (ECL) and organically treated montmorillonite (o-MMT). The polymerization is performed in bulk, at 165°C, i.e., below the melting point of the resulting APA6, the reaction time being in the range of 10–15 min. The o-MMT content is varied in the 0.5–10% range. X-ray diffraction (XRD) and transmission electron microscopy (TEM) show that exfoliated NPC can be produced with clay loads of 0.5–1.0%. Larger clay amounts lead to various degrees of intercalation of the MMT layers. FT-IR imaging proves that all NPCs contain MMT aggregates with sizes in the 10–20 μm range. The formation of the matrix crystalline structure is followed directly by performing AAROP of an activated ECL/o-MMT blend in a synchrotron beamline. Irrespective of the o-MMT type and concentration, it is the α-PA6 that forms first and in larger amounts. The γ-PA6 polymorph can be found in predominating amounts only after melting and recrystallization of the already produced polymer matrix.
 J. Appl. Polym. Sci. 130: 1228–1238, 2013

KEYWORDS: X-ray; ring-opening polymerization; nanostructured polymers; polyamides; properties and characterization

Received 19 November 2012; accepted 11 March 2013; Published online 19 April 2013
DOI: 10.1002/app.39274

INTRODUCTION

Nanostructured polymer composites (NPCs) display significant improvement in important properties of the matrix polymer such as mechanical strength and stiffness, thermal stability and heat distortion temperature, flame retardancy, and gas barrier performance.[1,2] This makes them very useful in applications related to automotive parts, household electrical appliances, and food-packaging films.[3] As repeatedly recognized, the improvement of the properties of NPCs largely depend on their nanoscale structure, which includes: (i) homogeneous and random dispersion (exfoliation) of silicate layers; (ii) adequate interactions between the specific polymer molecules and the silicate platelets' surface; and (iii) appropriate influence of inorganic layers on the polymer conformation and morphology. For semicrystalline polymer matrices, in the latter case, the reinforcing silicate layers can induce polymorphism thus affecting the whole set of NPC properties.[4]

NPCs based on polyamide 6 (PA6) and montmorillonite (MMT) were developed and industrially manufactured by Toyota Research Group in 1985 and have rapidly gained industrial importance. Fully exfoliated PA6/MMT nanocomposites called also "hybrids" with best properties were first produced by ring-opening polymerization of ε-caprolactam (ECL) in the presence of organically treated MMT (o-MMT), i.e., by creating the polymer matrix *in situ*.[3,5,6] As standard preparative method Toyota scientists adopted the acid-catalyzed hydrolytic polymerization of ECL, no matter that it was quite slow (11–13 h per batch) and required maintaining the reaction mixture in the melt at 240–260°C.[7] They also tested an alternative method, namely the activated anionic ring opening polymerization of ECL (AAROP) but abandoned it by the late 1980s due to insufficient control on its rate and on the exfoliation in the final NPC.[3] It was, nevertheless, recognized that the AAROP could take place at temperatures far below the melting of the resulting PA6 (typically in the 150–180°C range) at rates being 10^3-10^7 greater than of the hydrolytic process.[8]

Nowadays the preparation of neat PA6 by AAROP is well studied and understood.[9,10] Strong bases such as metal caprolactamates are most often employed as initiators of the process and imide-group containing compounds (e.g., acyl lactams), as activators.[11,12] Changing the activator amount or its chemical composition not only influences the AAROP rate but also can result in PA6 materials with linear or star-shaped macromolecules possessing unusual mechanical and rheological properties,[13] as well as in flame retardant properties without any addition of fillers.[14]

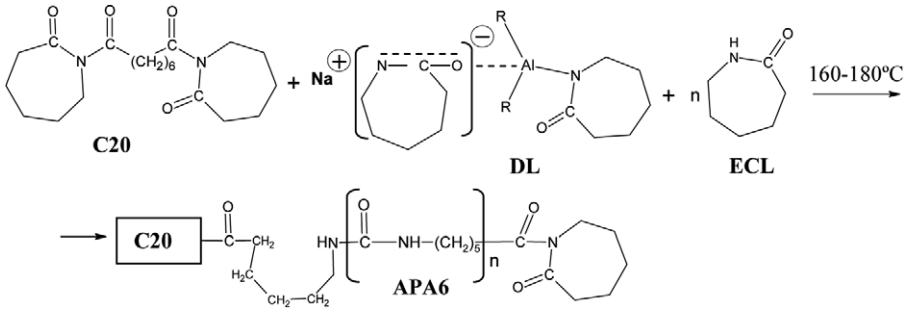

Scheme 1. Schematics of the chemical reactions and compounds in AAROP: C20, Bruggolen C20 (activator); DL, dicaprolactamato-bis-(2-methoxyethoxo)-aluminate, R = $OCH_2CH_2OCH_3$ (initiator); ECL, ε-caprolactam; APA6, anionic polyamide 6. The structure of DL is according to Ref. 33. The structure of C20 is based on own analyses.

There exist, however, only few studies on the PA6–MMT nanocomposites prepared by AAROP. Thus, according to Liu et al.[15] both pristine and organically treated MMT (o-MMT) were unsuitable for AAROP of ECL due to their severe inhibiting effect on the initiator–activator complex. Moreover, in view of the study of Yeong et al.,[16] the dispersion of o-MMT in ECL is expected to be poor due to insufficient *H*-bonding between them leading to impossibility for the monomer to penetrate the galleries of the clay and form exfoliated NPCs. Reportedly, in order to obtain PA6/MMT hybrids via AAROP one has to employ intercalation by ECL of pristine MMT in water followed by time- and labor-consuming drying procedures before polymerization.[17,18] Copolymer PA6/PA12–MMT nanocomposites were also prepared very recently using pristine Na-MMT clay.[19] Homoionic MMTs of the types Ca-MMT, Ba-MMT, and Mg-MMT were prepared from Na-MMT and used as fillers for PA6-based NPCs obtained by either AAROP or melt-mixing procedures.[20] In all cases, small fraction of exfoliated platelets was detected by TEM, tactoid splitting being weaker in melt-blended NPCs than in those by AAROP.

The influence of the clay reinforcements on the matrix polymorphic structure in PA6/MMT nanocomposites has been extensively reviewed.[4,21] It has been repeatedly recognized that in the presence of MMT platelets the γ-PA6 polymorph is predominantly formed.[22–25] Evidence was provided that, even when both γ- and α-crystals are present, the former ones are closer to the platelets' surface than the latter ones, corroborating the actual influence of clay on the preferred nucleation of γ-crystals.[26,27] γ-PA6 crystals have been shown to appear first during slow cooling from the quiescent melt before the development of α-crystals upon further cooling.[28] Several authors have reported that α-form crystals may be predominant over γ-crystals in the presence of MMT only under special conditions, depending on thermal history, and thermo-mechanical treatment.[29,30]

It should be noted that all of the above structural studies were made on PA6–MMT systems obtained either by the hydrolytic polymerization pathway or by melt processing. In both cases, the processing is carried out above the PA6 melting temperature. To the best of our knowledge, so far, there have been no systematic studies on the structure and morphology in NPCs prepared by solid-state AAROP, i.e., below the melting point of the matrix. Hence, in this study, we report on the preparation and properties of PA6-based NPCs obtained by solid-state AAROP of ECL in the presence of two commercial organically treated MMT brands. The main objective was to discuss the structural evolution in the composites (e.g., clay dispersion and PA6 polymorph content) as the solid-state AAROP advances and to try to relate it with the nanoclay type and concentration.

EXPERIMENTAL

Materials

The ε-caprolactam monomer (ECL) with reduced moisture content suitable for AAROP (AP-Nylon® caprolactam) was delivered from Brüggermann Chemical, Germany. Before use, it was kept under vacuum for 1 h at 23°C. As polymerization activator, Bruggolen C20P® from Brüggermann Chemical, Germany (C20) was used. According to the data sheet of the manufacturer, it contains 80 wt % of blocked di-isocyanate in ECL. The supposed chemical structure of C20 is presented in Scheme 1. The initiator sodium dicaprolactamato-bis-(2-methoxyethoxo)-aluminate (80 wt % in toluene) was purchased from Katchem and used without further treatment (Dilactamate®, DL, Scheme 1).

The nanoclay brands employed in this study were Cloisite 15A (CL15A) and Cloisite 20A (CL20A) manufactured by Southern Clay Products. They both represent natural MMT modified by dimethyl dihydrogenated tallow quaternary ammonium chloride and contain up to 2% of moisture. According to manufacturer's data, CL15A has a slightly higher modifier amount (125 meq/100 g versus 95 meq/100 g of CL20A) resulting in organic contents of 43 and 38%, respectively, measured by TGA. Both nanoclyas were dried for 2 h at 110°C in an oven and then immediately used.

Preparation of PA6–MMT Composites by *In Situ* AAROP

About 0.5 mol of ECL are molten in a 250 mL flask at 110°C under nitrogen flux and then the desired amounts of nanoclay are added at once. The mixture is energetically stirred at the same temperature until complete clay dispersion that took times typically up to 90 min. Then, 1.5 mol % of DL and 0.75 mol % of C20 are added. Upon homogenization, the reactive mixture is rapidly transferred into a rectangular mold (120 × 80 × 1.5 mm), which is then placed between the plates of a hot press heated at

165°C applying a mild pressure of 10 MPa. After 15 min, the temperature is gradually decreased at 10° min^{-1} demolding the sample at 35–40°C. All NPCs thus prepared displayed a degree of monomer conversion in the 97–99% range determined by Soxhlet extraction with methanol to constant weight.

Characterization Techniques

Most of the wide-angle X-ray scattering patterns (WAXS) in this study were registered at the Soft Condensed Matter Beamline (A2) of HASYLAB, Hamburg, Germany using synchrotron radiation with a wavelength fixed to 0.15 nm. The sample-to-detector distance was set at 90 mm, the diffraction patterns being registered by means of a MARCCD two-dimensional detector of Rayonix. The samples were studied in transmission mode with an exposure time of 25 s. A sample holder with incorporated heaters and cooling with compressed air was used allowing for controlled heating–cooling cycles in the 30–300°C range. For the in-beam AAROP study, a mixture of ECL with 1 wt % of CL20A was prepared as previously explained. Then, the initiator and activator were added and 0.4 g of the resulting mixture was placed into an aluminum capsule. The latter was affixed on the holder right in the optical path of the X-rays and the polymerization was performed in the synchrotron beamline. An Imago multichannel processor and program controller of JUMO GmbH (Germany) were used to regulate the sample temperature in heating and cooling. The difference between the read-out and real temperature was found to be 3–4°C at the heating rate of 20°C/min applied in this study. Corrections for background scattering, irradiated volume, and beam intensity were performed for each 2D pattern. For further data processing, a commercial software package was used.[31] Peak-fitting was applied in the linear WAXS patterns obtained after integration in the range between scattering angles 2θ of 3 and 40°. For some samples, a D8 diffractometer with $\theta/2\theta$ goniometer of AXS Bruker was employed with Cu $K\alpha = 0.154$ nm for taking of linear WAXS patterns at room temperature.

The FT-IR microscopy studies were performed in a Spotlight 300 IR (Perkin-Elmer) microscope with a dual mode array detector allowing for IR imaging and single-point spectra in the 4000–750 cm^{-1} range with a resolution of 5.0 μm. For this analysis, slices with a thickness of 12 μm were produced from the sample in a Leitz 1401 microtome (Wetzlar, Germany) using a glass blade.

Selected PA6/o-MMT nanocomposites were observed by TEM using a Zeiss 902A microscope, coupled with CCD camera Orius 1100. The observations were done on ultrathin sections (*ca.* 80 nm) cut at about −120°C with a Leica FC6 ultra microtome equipped with diamond knife. Before the observation, the sections were stained with RuO_4.

RESULTS AND DISCUSSION

The Polymerization Process

The chemistry of the activated anionic ring-opening polymerization (AAROP) of ECL is well-known since the early 1970s. Scheme 1 gives an idea of the accepted reaction mechanism summarized in a number of reviews.[9–11] Thus, AAROP, in this study, is initiated by the basic DL—an organo-aluminum compound that contains a stabilized caprolactamate anion. It is believed that in DL the lactam anion is with decreased nucleophility due to coordination of the Al atom with the lactam carbonyl oxygen leading to delocalization of the negative charge.[32] This makes DL a slower AAROP initiator as compared to the simple sodium caprolactamate.

The activator C20 contains two preformed imide links C(O)–N–C(O), in the presence of which polymerization starts directly with the propagation reaction.[33] Having in mind the amount of activating imide groups in C20 and the initiating caprolactamate anions in DL, the mole ratio of C20:DL was always at 1:2. After a number of optimization experiments, the AAROP temperature was set to 165°C, which produced the neat APA6 samples or the PA6/o-MMT composites with 97–99% degree of conversion within 15–20 min depending on the DL and C20 concentration.

The average viscometric molecular weight M_v of the neat APA6 was determined by intrinsic viscosity measurements in 97% sulfuric acid at a concentration of 0.2 g/L with a suspended level Ubbelohde viscometer thermostatted at 25°C. Using the Mark–Houwing equation with $K = 4.10^{-3}$ and $\alpha = 0.7$ for PA6,[34] M_v values in the range of 32,000–35,400 were obtained. This confirms the preparation of a high molecular APA6. The APA6/MMT composites were not completely soluble in sulfuric acid. Having in mind that the clay did not affect the time duration or the chemistry of AAROP, the molecular mass of the APA6/o-MMT composites is expected to be close to that of the neat APA6.

To further confirm the high molecular weight of the resulting APA6 composites, the sample containing 1% of CL20A was subjected to DSC in heating mode at 10° min^{-1}. A melting peak at 221.2°C was obtained showing an enthalpy of melting $\Delta H_m = 95.1$ J/g corresponding to a crystallinity index of 46.4%. The value of the enthalpy of fusion of a 100% crystalline PA6 $\left(\Delta H_m^{\infty}\right)$ was taken as 204.8 J/g.[35]

Nanoclay Dispersion Prior and After AAROP

The evolution of the basal peak of neat o-MMT from CL20A and CL15A (curves 1a and b), in their mixtures with ECL (ECL:o-MMT = 98:2 wt %) after different homogenization times at 110°C is shown in Figure 1. Curves 2–4 with both o-MMT types were produced with samples taken after 10, 30, and 90 min of mixing, cooling down to room temperature, and obtaining the WAXS pattern at 30°C. After mixing for 90 min, the catalytic system comprising 1.5 mol % of DL and 0.75 mol % of C20 is added and the reaction mixture is transferred to a mold where AAROP takes place at 165°C. Curves 5a and b are the WAXS patterns of the final NPCs.

As seen from Figure 1, the two neat o-MMT display different positions of the 001 basal peak corresponding to 25.5 Å (CL20A) and 30.5 Å (CL15A). This is in good agreement with the lesser amount of organic modifier in the former MMT type determining a smaller height of the galleries. Both nanoclay brands display also peaks in the 2θ range of 6–7° (12.5–13 Å) corresponding to the d_{001} of certain amounts of pristine MMT, not intercalated with organic modifier. Judging from the decrease and eventual complete disappearance of the basal peaks of organically modified and pristine MMT, as the mixing time

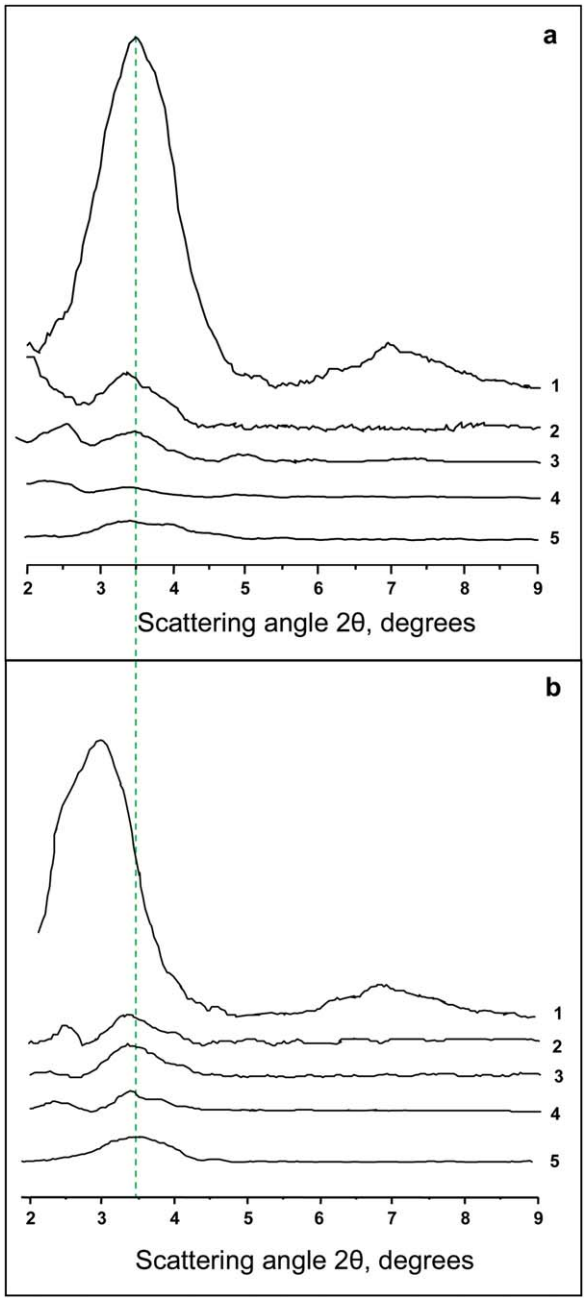

Figure 1. WAXS patterns of ECL/MMT mixtures (2/98 wt %) containing (**a**) ECL–CL20A and (**b**) ECL–CL15A after various mixing times at 110°C: 2 – 10 min; 3 – 30 min; 4 – 90 min; 5 – sample 4 after AAROP. Curves 1a and 1b present the patterns of the two neat MMT brands. WAXS patterns are obtained in a D8 diffractometer at 30°C. Curves are shifted along the *y*-axis. For more details, see the text. [Color figure can be viewed in the online issue, which is available at wileyonlinelibrary.com.]

increases [Figure 1(a), curves 2–4], it can be concluded that melt mixing of the ECL/CL20A system results in a complete dispersion to single nanoclay platelets. This was not the case with the ECL/CL15A mixtures [Figure 1(b), curves 2–4]. Until the 90th min of the mixing duration, the CL15A basal peak at 3.5° persisted showing a constant intensity and a shift toward larger 2θ values as compared to the neat nanoclay. Hence, it can be concluded that CL15A was not completely dispersed into single platelets during its mixing with ECL. A possible explanation of this fact can be the larger amount of organic modifier in this nanoclay brand that impedes its full dispersion in the relatively hydrophilic ECL. Notably, during the first 10 min of melt mixing of the ECL/2% CL15A system, a shift of the basal peak is observed corresponding to a gallery height decrease of 5 Å. This observation could be related to conformational changes of the long chain organic modifier or even to removal of some of it from the nanocly galleries. Logically, after AAROP in this system, an intercalated PA6/MMT composite is formed.

In spite of the fact that 2 wt % CL20A was completely dispersed in the molten ECL, the AAROP of this mixture resulted in a NPC that displayed a broad, low-intensity peak between 3–4° (curve 5a). Its presence suggests that the full dispersion of the clay in ECL before AAROP is not a guarantee for the production of fully exfoliated composite. Apparently, the polymerization may cause partial inverse aggregation of MMT platelets. The intensity of the respective diffraction peak, however, is comparable to the noise levels of the diffractometer used. To enable more rigorous structural conclusions, synchrotron WAXS experiments were performed.

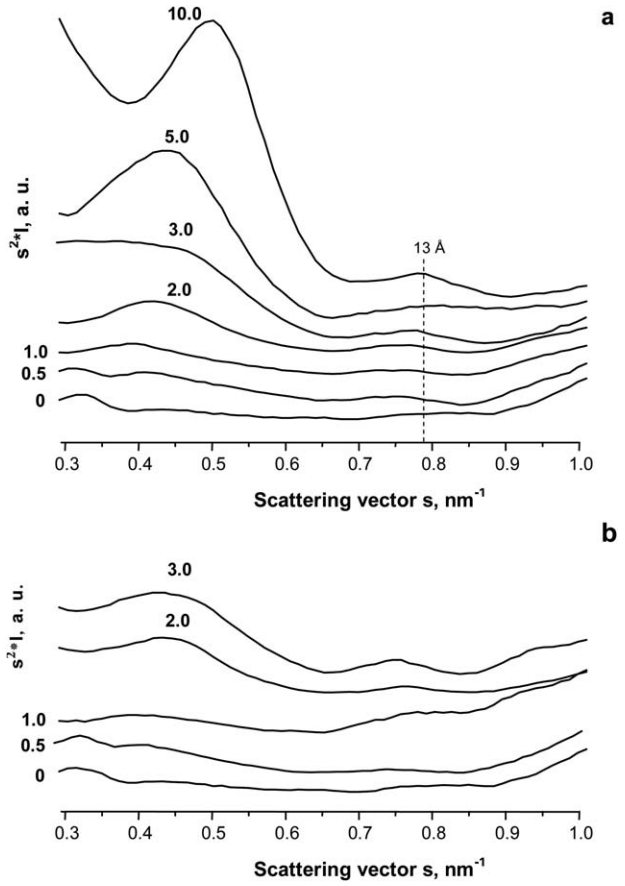

Figure 2. WAXS patterns of PA6/o-MMT composites (low *s*-values region) containing different amounts of: (**a**) CL20A and (**b**) CL15A. The numbers to curves correspond to the MMT concentrations in wt % in respect to APA6. The Lorentz-corrected patterns are shifted along the *y*-axis for clearness. Exfoliated MMT is observed with CL20A and CL15A concentrations of 0.5 and 1.0%.

Applied Polymer SCIENCE

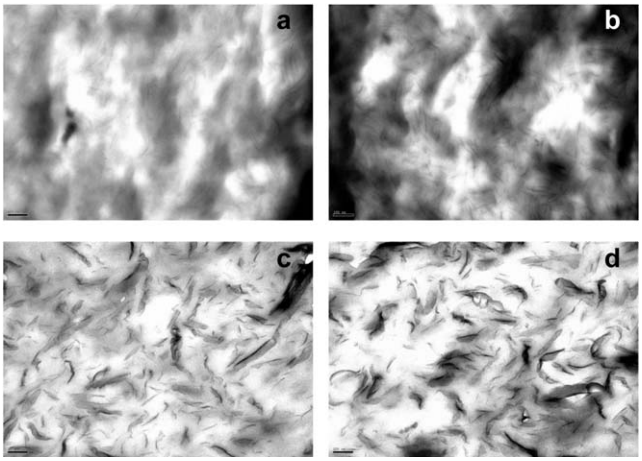

Figure 3. TEM images of PA6/CL20A NPCs with different amounts of MMT: (a) - 0.5%; (b) - 1.0%; (c) - 3.0%; (d) - 5%. The scale bar in all images corresponds to 100 nm. With 0.5 and 1.0% single MMT lamellae are observed; higher clay loads result in intercalated tactoid structures.

Figure 2 shows the low *s*-values region of WAXS patterns of PA6/o-MMT composites, in which the CL20A and CL15A vary in a broad range. To enable comparison, the WAXS profile of the neat PA6 is also presented (curves 1a and 1b). It can be seen that irrespective of the Cloisite brand, the NPCs with 0.5% (curves 2a and 2b) and 1.0 % of clay (3a and 3b) do not display basal reflection and can be therefore considered exfoliated. As expected, increasing the MMT content led to aggregation and formation of intercalated PA6/MMT composites. Thus, the composites with 2 and 3% CL20A show a broad reflection with d_{001} of 20–29 Å corresponding to basal long spacings of silicate layers with different stages of intercalation (curves 4a and 5a). This reflection is somewhat more intense in the systems containing CL15A (curves 4b and 5b). AAROP of ECL in the presence of 5 and 10% of CL20A produced composite materials (curves 6a and 7a) with increasing aggregation of clay layers showing gallery heights of 23 and 20 Å , respectively. In these two profiles, the d_{001} reflection of the pristine MMT at *ca.* 13 Å is also observed.

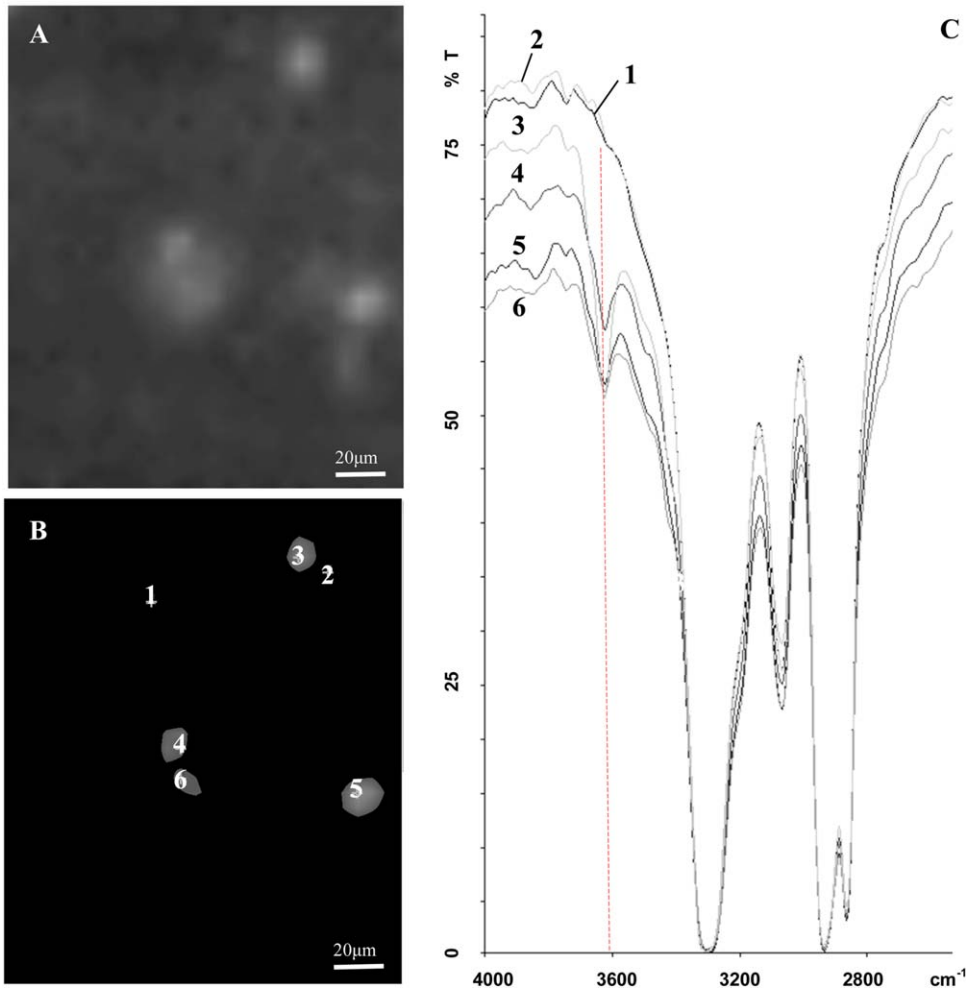

Figure 4. FTIR gray scale maps of a PA6/CL20A NPC with 1 wt % of MMT. White corresponds to 100% MMT, black – to 100% PA6. (**A**) Minimum threshold of the MMT band sensitivity; (**B**) Fixed higher threshold of the MMT signal; (**C**) FTIR spectra (% transmission versus wavelength) taken in selected points of the microscopic image. The numbers of the spots and of the spectra coincide. Micron-size agglomerations are observed even in samples exfoliated according to WAXS. [Color figure can be viewed in the online issue, which is available at wileyonlinelibrary.com.]

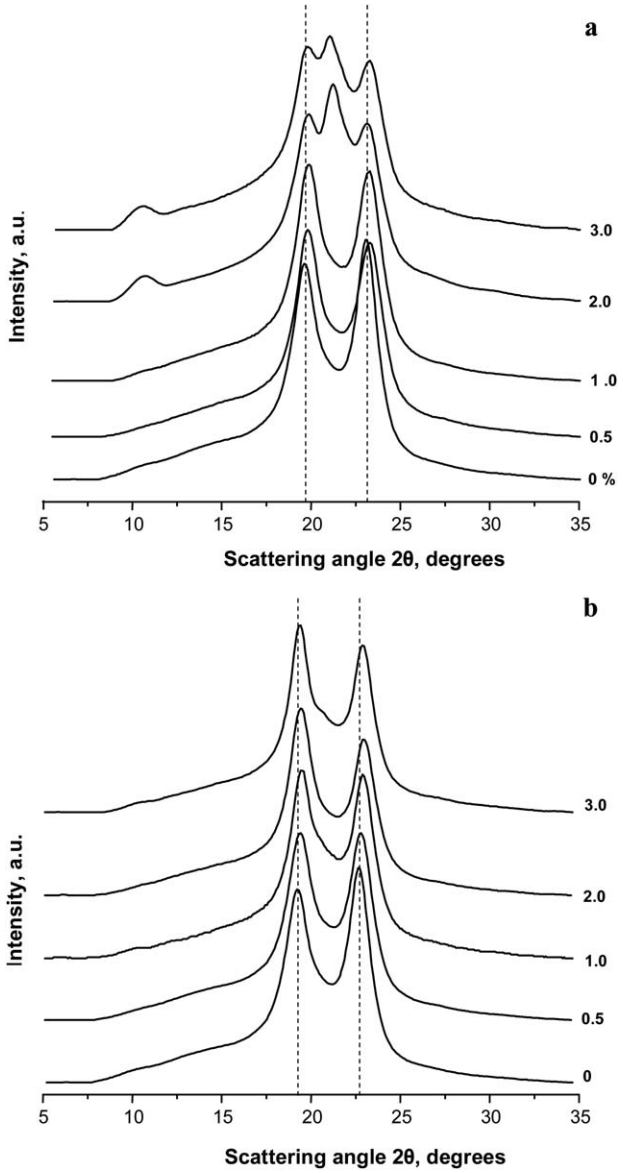

Figure 5. Synchrotron WAXS profiles of as-prepared PA6/o-MMT composites (2θ region above 5°, irradiation at 30°C) containing different amounts of: (**a**) CL20A and (**b**) CL15A. The numbers to curves correspond to the MMT concentrations in wt % in respect to APA6. The patterns are shifted along the *y*-axis for clarity. Predominant α-PA6 polymorph is observed in all composites with the exception of the APA6/CL20A systems with 2 and 3% MMT. For more information see Tables I and II.

The WAXS profiles in Figure 2 allow the conclusion that exfoliated NPCs (hybrids) via AAROP can readily be produced with clay concentrations below 2 wt %. Intermediate amounts of 2 and 3% lead to intercalated PA6/MMT materials, whereas clay loads of 5 and 10% CL20A resulted in pronounced aggregation of the MMT component—both organically treated and pristine. Therefore, the dispersion of the reinforcements in NPCs produced by solid-state AAROP follow the same trend as in the composites obtained by the hydrolytic method.

Contrary to some earlier studies,[15,17] no inhibition effect of o-MMT upon the AAROP was observed. This fact can be explained with the above-mentioned (Scheme 1) delocalization of the negative charge of the caprolactamate anion in DL that makes it a slower initiator but, apparently, more stable to deactivation by acidic species than the commonly used simple ECL anion. In addition, DL was proved to be more stable to moisture,[33] which makes it more useful under industrial conditions.

The TEM images of selected PA6/CL20A composites with increasing MMT content (Figure 3) are in conformity with the WAXS studies. The samples with 0.5 and 1.0 wt % of MMT display homogeneous and random distribution of single silicate platelets with thicknesses close to 1 nm. In the NPCs with 3 and 5% clay, the distribution of the mineral component is still homogeneous, however stacking into thicker, sheet-like tactoide aggregates is observed.

The TEM images in Figure 3 visualize areas of only 1 μm^2. That is why an attempt was made to evaluate the micron-scale homogeneity of the exfoliated NPC with 1 wt % of CL20A. Figure 4 shows the gray scale maps of a FT-IR microscopic image of this nanocomposite over an area of 200 × 165 μm. The

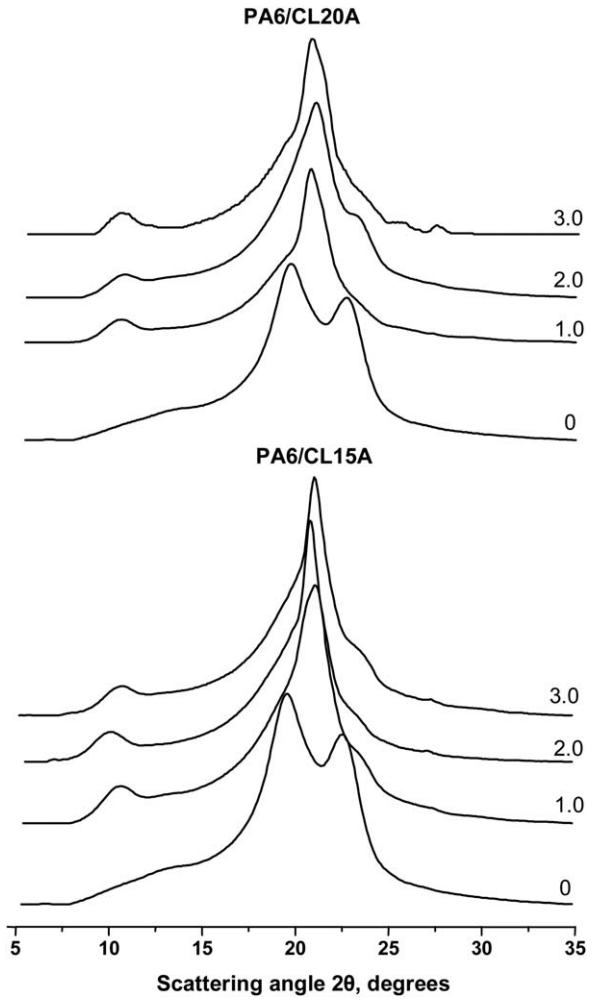

Figure 6. WAXS patterns of PA6/o-MMT composites in-beam melting after 5 min at 260°C and cooling down to 30°C. The numbers to curves correspond to the MMT concentrations in wt % in respect to APA6. For more information see Tables I and II.

Table I. Influence of the CL20A Content on the Crystalline Structure of the PA6 Matrix

CL20A content (wt %)	As prepared				After annealing at 200°C				After melting and recrystallization			
	Crystal-linity (%)	α (%)	γ (%)	α/γ	Crystallinity (%)	α (%)	γ (%)	α/γ	Crystallinity (%)	α (%)	γ (%)	α/γ
–	46.0	32.5	13.5	2.41	50.9	36.0	14.9	2.42	49.1	33.9	15.2	2.23
0.5	45.1	27.3	17.8	1.53	47.8	26.2	21.6	1.21	41.0	9.2	31.8	0.29
1.0	48.8	26.9	21.9	1.23	45.2	28,4	16.8	1.69	42.9	7.6	35.3	0.22
2.0	48.9	21.3	27.6	0.77	50.2	32.1	18.1	1.77	49.3	13.9	35.4	0.39
3.0	45.4	17.5	27.9	0.63	49.0	22.4	26.6	0.94	49.7	8.7	31.0	0.28

mapping is based on the IR band of non-associated OH-group of MMT at 3631 cm^{-1} (white) and the Amid 1 C=O band of PA6 at 1668 cm^{-1} (black).[36] The image in Figure 4(A) is produced with maximum sensitivity in respect to the MMT signal. In the Figure 4(B), this sensitivity is decreased by 12%, which eliminates the weak signals of the finely distributed MMT component and visualizes only the aggregates with sizes of above 2–3 μm. The comparison of these two images shows that in this exfoliated NPC at micrometer length scale there exist several domains in the 15–20 μm range representing MMT aggregates. The number of each spot in Figure 4(B) corresponds to the FT-IR spectrum number in Figure 4(C). As expected, between the domains of aggregation (spots 1 and 2), no signal for the OH-groups of MMT can be resolved. At the same time, clear OH-peaks at *ca.* 3650 cm^{-1} are observed in spots 3–6 confirming their relation to the MMT component. This means that in NPCs with well-dispersed inorganic nanoclays considered exfoliated at nanometer length scale, micrometric aggregates may be found if large enough sample areas are observed. This aggregation may limit the improvement of the mechanical properties of the NPCs especially if relatively hard matrices as PA6 are used.[37]

Crystalline Structure of the PA6 in the Presence of MMT

The presence of silicate layers in the PA6 matrix is known to influence the conformation of polyamide molecules and their arrangement. It modifies the overall crystallinity index as well as the amount of α- and γ-polymorphs, which could change the whole set of NPC properties. MMT type, its content and the temperature of the AAROP (or that of some subsequent annealing) are the most important factors that control the crystalline structure of the matrix PA6.

Figure 5 displays the linear WAXS profiles in the 2θ range of 5–35° of as-prepared PA6/o-MMT composites comprising the two Cloisite brands that vary in the range between 0.5 and 3 wt %. The AAROP was performed at 165°C as indicated in the "Experimental" section. The pattern of the neat matrix prepared under the same conditions is also presented for comparison. It can be seen that in the NPCs with 0.5 and 1 wt % of CL20A [Figure 5(A)] and in all CL15A modified samples [Figure 5(B)], the monoclinic α-PA6 polymorph is predominant, as is in the neat PA6. The α-PA6 characteristic reflections with 2θ values of 19.7 and 23° correspond to the α_{200} e $\alpha_{002/202}$ crystal planes formed between adjacent chains by van der Waals forces or *H*-bonds, respectively. In the NPCs with 2 and 3%, CL20A larger amounts of γ-PA6 are observed. This polymorph displays two almost coinciding peaks for the γ_{001} and γ_{200} crystal planes that appear between the reflections of the α-polymorph. In addition, these two samples reveal clear γ_{020} reflections around $2\theta = 10°$ (*b*-axis is the chain axis).

Deconvolution of all WAXS profiles in Figure 5 was performed as indicated previously[38,39]and the results for total crystallinity, content of α- and γ-PA6, as well as of the relation between the two crystalline forms were calculated (Tables I and II). In all as-prepared NPCs (with the exception of the samples with 2 and 3% of CL20A), the ratio $\alpha/\gamma > 1$. The total crystallinity index of the NPCs in this series does not depend on the MMT type or concentration, which was reported previously in both anionic[17] and with melt-blended[40] PA6-MMT composites. In this study, the total crystallinity remains in the range of 44–49%, which is close to that of the neat PA6 (46%). It is the α/γ that changes significantly—from 2.5 with the neat PA6 to 1.5—1.0 for the majority of the NPCs studied. In all these

Table II. Influence of the CL15A Content on the Crystalline Structure of the PA6 Matrix

CL15A content (wt %)	As prepared				After annealing at 200°C				After melting and recrystallization			
	Crystallinity (%)	α (%)	γ (%)	α/γ	Crystallinity (%)	α (%)	γ (%)	α/γ	Crystallinity (%)	α (%)	γ (%)	α/γ
-	46.0	32.5	13.5	2.41	50.9	36.0	14.9	2.42	49.1	33.9	15.2	2.23
0.5	46.0	24.5	21.5	1.14	49.1	30.4	18.7	1.63	47.9	10.1	37.8	0.27
1.0	46.7	23.6	23.1	1.02	48.2	29.1	19.1	1.52	48.8	9.6	38.2	0.25
2.0	42.9	23.2	19.7	1.18	44.0	27.6	16.4	1.68	43.1	13.0	30.1	0.43
3.0	44.4	27.0	17.4	1.55	46.2	27.8	18.4	1.51	50.0	9.2	40.8	0.23

samples, the two reflections of the α-polymorph are very symmetric. This finding suggests unconfined crystallization both along the plane formed by *H*-bonded chains and the plane of the van der Waals forces. Such an observation disagrees with previous results[41] obtained with a melt-blended PA6–MMT composite. In such systems, the presence of MMT reportedly always led to predominance of the γ-PA6 crystals.[18,26,27,40] The presence of large γ-PA6 amounts was even considered a proof for exfoliation of the nanoclay.[18] As evident from Figure 5 and Tables I and II, in the exfoliated PA6/o-MMT samples with 0.5 and 1.0 wt % of clay produced via solid-state AAROP (i.e., below T_m of the forming PA6), both polymorphs are formed but the amount of the α-crystals is larger or at least close to that of the less stable γ-form.

To clarify this apparent contradiction with the previous results on PA6 polymorphism in the presence of MMT, PA6/o-MMT composites with CL20A (Table I) and CL15A (Table II) were annealed at 260°C (Figure 6) and at 200°C (Figure 7). These tables and figures show evidence that in clay composites made by solid-state AAROP of ECL it is the thermal history of the sample and not the type or even the concentration of the MMT component that governs the appearance of a predominant amount of the γ-PA6 phase. Thus, annealing the NPCs for short times at 200°C, i.e., above the temperature of Brill transition, leads to an additional increase of the α-PA6 content in all samples, including those with 2 and 3% of CL20A. The α/γ relation changes in favor of the γ-polymorph reaching values around 0.3 only after melting at 260°C and recrystallization of the matrix material. This observation agrees with all previous systematic studies on the polymorphism in PA6/MMT composites since they were performed in samples produced by methods involving melting of the matrix material—*in situ* hydrolytic polymerization in the melt or melt compounding of PA6 with MMT in an extruder or mixer. Evidently, the MMT layers are really strong γ-phase nucleating agent only in the recrystallization of molten, already existing PA6. In this study, the PA6 matrix was produced at 165°C, far below its T_m. These conditions apparently do not impede the formation of the more thermodynamically stable α-polymorph, irrespective of the presence of exfoliated, homogeneously distributed silicate monolayers, proved in the NPCs with 0.5 and 1.0% o-MMT.

Figure 8 shows the evolution of the *d*-spacings in the two polymorphs of the PA6 matrix as a function of the CL20A (a, b) or CL15A content (c, d) in the as-prepared samples and after melting at 260°C and recrystallization. It seems that in the as-prepared samples the *d*-spacing of the α(200) and α(002/202) reflections are less sensitive to the MMT concentration than those of the γ(001), γ(200), and especially of the γ(020). This observation might have something to do with the supposition that the γ-PA6 is more likely to form at the MMT/matrix interface.[26,27] Melting and recrystallization result in smaller fluctuations in the *d*-spacing values, slightly stronger in the CL20A containing NPCs. This o-MMT brand contains less organic modifier and therefore the nucleating silicate layers might interact more directly with the matrix PA6.

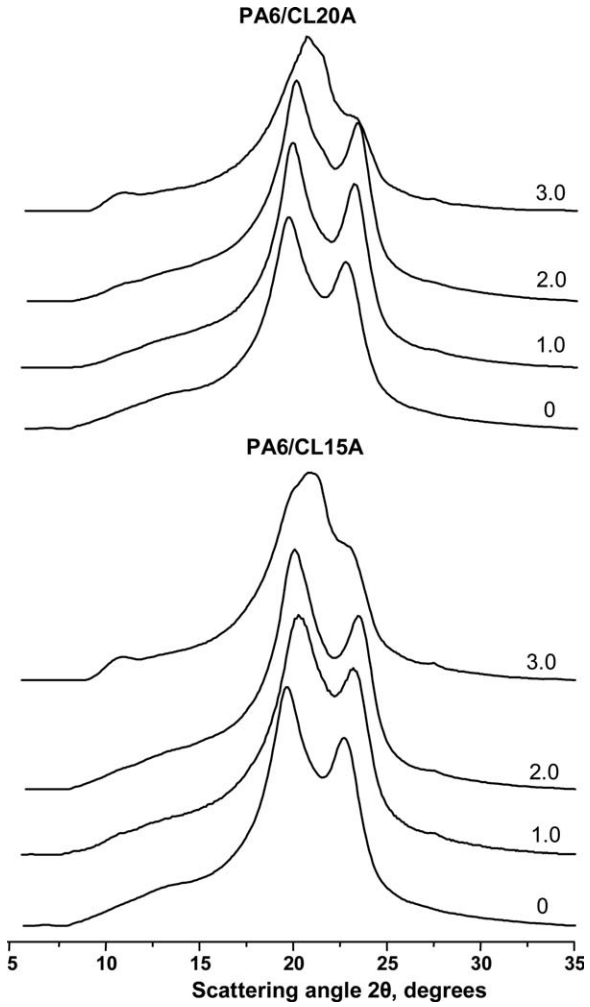

Figure 7. WAXS patterns of PA6/o-MMT composites after in-beam annealing for 5 min at 200°C. The numbers to curves correspond to the MMT concentrations in wt % in respect to APA6.

Evolution of the Matrix Nanostructure During In-Beam Monitoring of AAROP

In order to explain more rigorously the genesis of PA6 polymorphs during the solid-state AAROP in the presence of o-MMT, the evolution of the crystalline structure of ECL during its transformation into PA6 was monitored. To the best of our knowledge, such a measurement has not been performed so far. Thus, a mixture of ECL/1 wt % of CL20A was stirred until complete dispersion and then activated and initiated as explained in the Experimental part. About 0.4 g of this mixture was placed into an Al capsule similar to those used in DSC measurements and tightly closed by cramping. It was attached to a sample holder and irradiated with high intensity synchrotron X-rays in WAXS mode. The temperature was kept at 165°C in order to allow for the AAROP to take place in-beam. Every 30 s 2D WAXS images were taken, the most representative being shown in Figure 9, rows 1 and 2. It should be mentioned that the Al foil of the capsule is transparent for the synchrotron X-rays. The WAXS reflections of Al appeared at $2\theta > 38°$, i.e., outside the range of the ECL and APA6 peaks. After AAROP

Applied Polymer SCIENCE

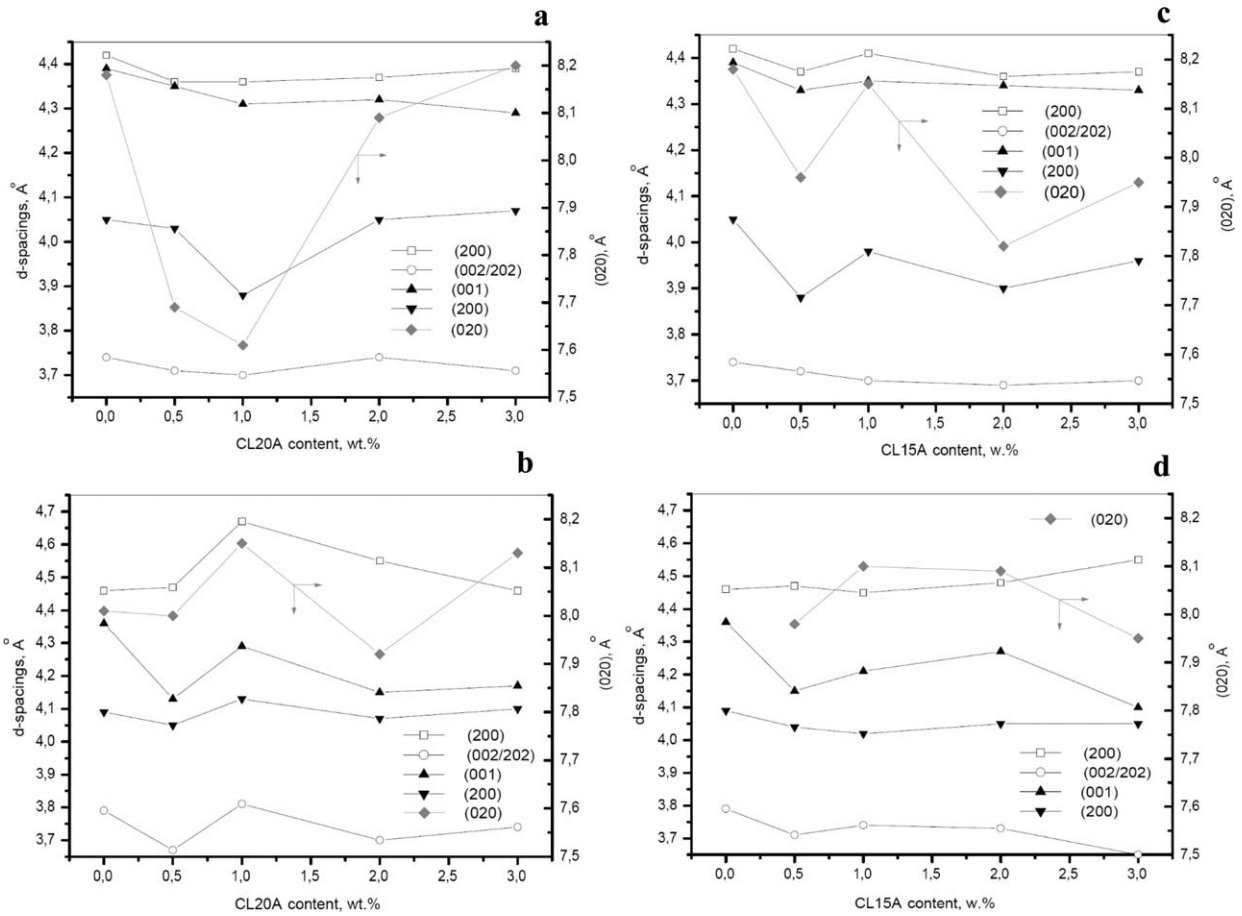

Figure 8. *d*-Spacings evolution of the PA6 matrix in NPCs reinforced by: (**a**) CL20A, as-prepared; (**b**) CL20A, recrystallized; (**c**) CL15A, as-prepared; (**d**) CL15A, recrystallized. Open symbols relate to the crystalline planes of the α polymorph; solid symbols - to those of the γ polymorph.

completion, WAXS images were also obtained at 30°C after annealing at 200°C and at 30°C after melting at 260°C. Thereafter, the linear WAXS profile was produced and analyzed (Figure 10).

Polymerization times in the 4–8 min range result in WAXS reflections that can only be associated with structural transformations in the ECL monomer related to strong intensity decrease and disappearance of certain diffraction peaks, especially above $2\theta = 20°$. At the same time, the group of reflections in the 16–18° range presented from the beginning of the polymerization is maintained. It should be noted that the profiles in Figure 10 at 4, 6, and 8 min are typical of low molecular weight, fully crystalline samples without any diffuse scattering of amorphous material. The latter appears in the sample with 10 min at 165°C, which is the first indication of polymer formation. At the same time, this sample displays incipient Debye rings of the α-polymorph (Figure 9) at 2θ values of *ca.* 18 and 23° (Figure 10). At the 12 min of AAROP, the system does not contain anymore the narrow crystalline ECL peaks between 8 and 16°, which could be considered a proof for polymerization completion. Instead, this WAXS profile shows an amorphous halo and the well-known structure with predominant well-expressed α-crystals already known from Figure 5.

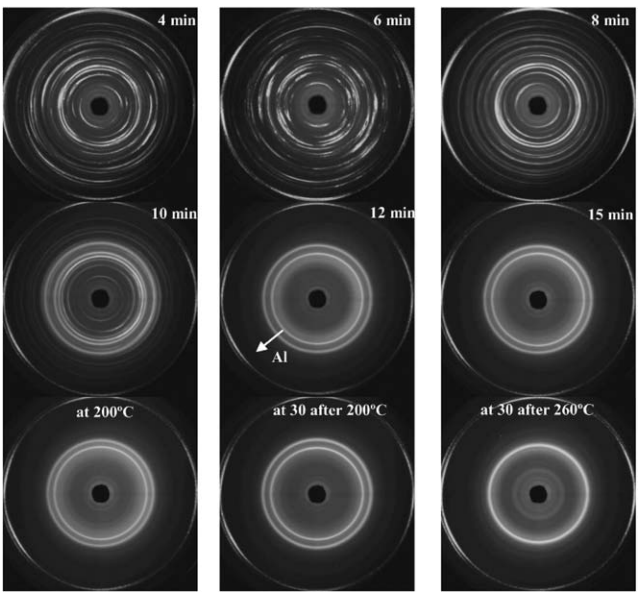

Figure 9. Synchrotron WAXS in-line monitoring of the structure evolution during AAROP in an ECL/CL20A mixture (99:1) as a function of reaction time at 165°C (top and middle rows), and the subsequent annealing of the resulting NPC (bottom row). The utmost external circular reflection belongs to the Al capsule in which the polymerization takes place.

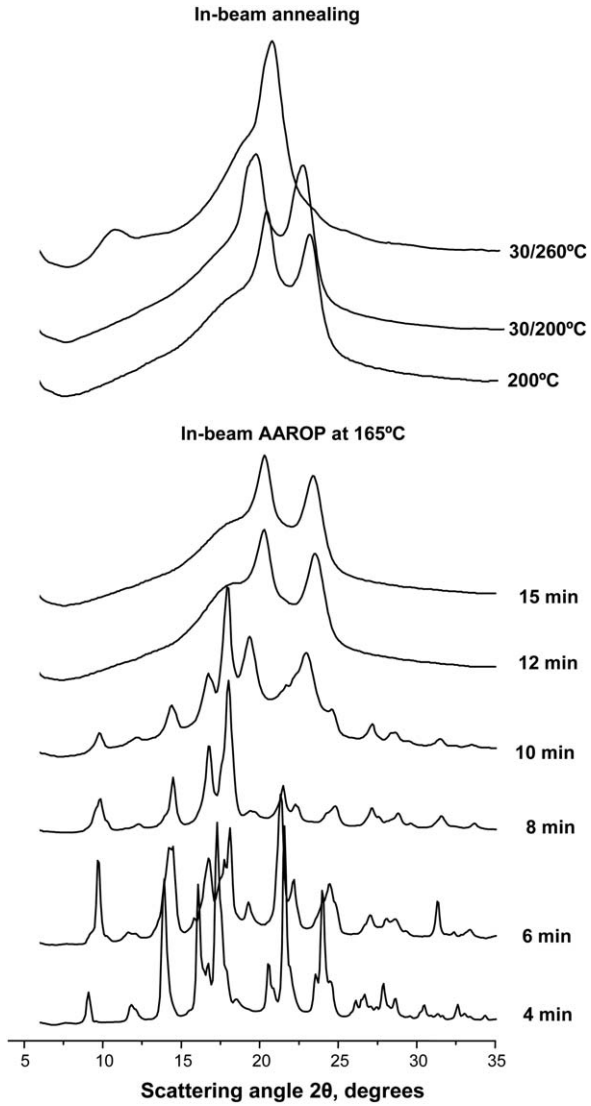

Figure 10. In-line monitoring of the structure developments during AAROP in an ECL/CL20A mixture (99:1%) as a function of reaction time and the subsequent annealing of the resulting NPC. The WAXS patterns are obtained by slicing 2D WAXS images in Figure 9 and are shifted along the *y*-axis for clarity. The two reflections of the α-polymorph appear after 10 min of AAROP and become evident within the next 5 min reaction time.

Extending the AAROP time to 15 min does not result in any structural change in the PA6 matrix in this NPC, and neither did the annealing at 200°C. It should be noted that, judging from the intensity of the diffuse diffraction peak in the PA6 matrix in Figure 10, the in-beam AAROP apparently produced polymer of lower total crystallinity, as compared to the regular NPC samples previously studied (Tables I and II). As to the polymorph content, however, the in-beam solid-state AAROP of an ECL/o-MMT mixture confirmed completely that it is the α-polymorph that forms first and in larger amounts. As expected, a well-expressed γ-PA6 polymorph was produced only after melting and recrystallization of the PA6 matrix in the presence of the silicate component (Figure 10, 30°C after melting).

CONCLUSIONS

This study proves that PA6-based composites can be successfully prepared by solid-state AAROP of ECL in the presence of 0.5 to 10% wt % of Cloisite 15A and Cloisite 20A clays representing organically treated MMT. All neat APA6 and composite samples were synthesized within the 10–15 min, with high molecular weights and without any signs of catalyst system deactivation. It was demonstrated that the composites with 0.5 and 1.0% clay reinforcement can be considered exfoliated PA6/o-MMT hybrids; higher clay loads result in materials with intercalated (tactoid-containing) MMT domains.

Notably, even NPCs exfoliated at nanoscale as revealed by WAXS and TEM are not completely homogeneous in terms of clay distribution. The FT-IR imaging showed the presence of clay agglomerates at micron scale.

Unlike the other methods for preparation of PA6/MMT nanocomposites including matrix melting, the solid-state AAROP produced PA6 matrices with predominant concentration of the α-crystalline phase. The latter was not affected by the type or concentration of the MMT used but only by the thermal conditions of AAROP.

It was demonstrated that under the conditions of this study, predominantly α-PA6 is formed as a result of simultaneous polymerization and solid-state crystallization (below T_m) and not as a result of a phase transition. Significant amounts of γ-PA6 could be formed in the NPCs only after melting and recrystallization of the already existing PA6 matrix.

ACKNOWLEDGMENTS

The authors gratefully acknowledge the financial support of HASYLAB at DESY (Grant Number II-07–011EC). N.D. is grateful to the Fundação para a Ciênica e Tecnologia (FCT), Portugal for supporting her research by the post-doctoral award SFRH/BPD/45252/2008, co-financed by QREN-POPH program of EU.

REFERENCES

1. Giannelis, E. P. *Adv. Mater.* **1996**, *8*, 29.
2. Usuki, A.; Hasegawa, N.; Kato, M. *Adv. Polym. Sci.* **2005**, *179*, 135.
3. Okada, A.; Usuki, A. *Macromol. Mater. Eng.* **2006**, *291*, 1449.
4. Li, Y.; Shimizu, H. *J. Polym. Sci. Part B: Polym. Phys.* **2006**, *44*, 284.
5. Kojima, Y.; Usuki, A.; Kawasumi, M.; Okada, A.; Kurauchi, T.; Kamigaito, O. *J. Polym. Sci. Part A: Polym. Chem.* **1993**, *31*, 983.
6. Usuki, A.; Kojima, Y.; Kawasumi, M.; Okada, A.; Kurauchi, T.; Kamigaito, O. *Polymer* **1990**, *31*, 651.
7. M. Kawasumi, M. Kohzaki, Y. Kojima, A. Okada, O. Kamigaito (Toyota Chuo Kenkyuusho). US Patent 4,810,734, March 7 **1989**.
8. Kohan, M. I. Nylon Plastics; Wiley: New York, **1973**, p 213.

9. Sebenda, J. In Polymerization of Heterocyclics; Vogl, O., Furukawa J., Eds.; Marcel Dekker: New York, **1973**; p 153.
10. Sekiguchi, H. In Ring Opening Polymerization; Ivin, K. J., Saegusa T., Eds.; Elsevier: New York, **1984**; Vol. *2*, p 809.
11. Roda, J. In Handbook of Ring-Opening Polymerization; Dubois, P., Coulembier, O., Raquez, J-M., Eds.; Wiley-VCH: Wincheim, **2009**; Chapter 7, p 177.
12. Gabbert, J. D.; Hedrick, R. M. *Polym. Process. Eng.* **1986**, *4*, 359.
13. Mathias, L. J.; Sikes, A. M. In Cross-linked Polymers; Dickie R., Ed.; ACS Symposium Series: Washington, DC, **1988**; p 66.
14. Mateva, R.; Dencheva, N. *J. Polym. Sci. Part A: Polym. Chem.* **1992**, *30*, 1449.
15. Liu, M. G.; Song, Q.; Zhou, C. X. In PA6 Nanoclay Composites via Anionic Polymerization, Proceedings of 2004 National Symposium of Polymer Materials Science and Engineering of China, Shanghai, China, October 2004, pp 241–242.
16. Yeong, S. C.; Hyeong, T. H.; In, J. C. *Chem. Mater.* **2004**, *16*, 2522.
17. Liu, A.; Xie, T.; Yang, G. *Macromol. Chem. Phys.* **2006**, *207*, 701.
18. Liu, A.; Xie, T.; Yang, G. *Macromol. Chem. Phys.* **2006**, *207*, 1174.
19. Cabrera Álvarez, E. N.; Ramos de Valle, L. F.; Rodriguez González, E. J.; Soriano-Corral, F.; Díaz de León, R. E. *J. Nanomater.* **2012**, doi: 10.1155/2012/487948.
20. Kadlecová, Z.; Puffr, R.; Baldrian, J.; Schmidt, P.; Roda, J.; Brozek, J. *Eur. Polym. J.* **2008**, *44*, 2798.
21. Miri, V.; Elkoun, S.; Peurton, F.; Vanmansart, C.; Lefebvre, J.-M.; Krawczak, P.; Seguela, R. *Macromolecules* **2008**, *41*, 9234.
22. Kojima, Y.; Usuki, A.; Kawasumi, M.; Okada, A.; Kuraichi, T.; Kamigaito, O.; Kaji, K. *J. Polym. Sci. Part B: Polym. Phys.* **1994**, *32*, 625.
23. Medellin-Rodriguez, F. J.; Burger, C.; Hsiao, B. S.; Chu, B.; Vaia, R.; Philips, S. *Polymer* **2001**, *42*, 9015.
24. Nair, S. S.; Ramesh, C. *Macromolecules* **2005**, *38*, 454.
25. Bertmer, M.; Wang, M.; Kruger, M.; Blumich, B.; Litvinov, V. M.; van Es, M. M. *Chem. Mater.* **2007**, *19*, 1089.
26. Lincoln, D. M.; Vaia, R. A.; Wang, Z.G.; Hsiao, B. S.; Krishnamoorti, R. *Polymer* **2001**, *42*, 9975.
27. Wu, Q.; Liu, X.; Berglund, L. A. *Polymer* **2002**, *43*, 2445.
28. Ibanes, C.; de Boissieu, M.; David, L.; Seguela, R. *Polymer* **2006**, *47*, 5071.
29. Fornes, T. D.; Paul, D. R. *Polymer* **2003**, *44*, 3945.
30. Espinosa, Z. A.; Rodriguez, M. F. J.; Stribeck, N.; Camarillo, A. A.; Diaz, V. S.; Hsiao, B. S.; Chu, B. *Macromolecules* **2005**, *38*, 4246.
31. POLAR, version 2.7.3; Copyright (c) 1997–2008 by Stonybrook Technology and Applied Research, Inc, USA.
32. Veith, C. A.; Cohen, R. E. *Makromol. Chem. Macromol. Symp.* **1991**, *42/43*, 241.
33. Dan, F.; Vasiliu-Oprea, C. *Colloid. Polym. Sci.* **1998**, *276*, 483.
34. Mateva, R.; Delev, O. *Polym. J.* **1995**, *27*, 499.
35. Brandrup, J.; Immergut, R. H. Polymer Handbook, 2nd ed.; Wiley: New York, **1975**.
36. Motovilin, M.; Denchev, Z., Dencheva, N. *J. Appl. Polym. Sci.* **2011**, *120*, 3304.
37. Schaefer, D. W.; Justice, R. S. *Macromolecules* **2007**, *40*, 8501.
38. Samon, J. M.; Hsiao, B. S. *Polymer* **2000**, *41*, 2169.
39. Dencheva, N.; Nunes, T.; Oliveira, M. J.; Denchev, Z. *Polymer* **2005**, *46*, 887.
40. Lincoln, D. M.; Vaia, R. A.; Krishnamoorti, R. *Macromolecules* **2004**, *37*, 4554.
41. Xie, S.; Zhang, S.; Liu, H.; Chen, G.; Feng, M.; Qin, H.; Wang, F.; Yang, M. *Polymer* **2005**, *46*, 5417.